applied optics

# Optical design of a short-wave infrared prism-grating imaging spectrometer

Jianjun Chen,[1,2] Jin Yang,[1] Jianan Liu,[1,2] Jianli Liu,[1,2] Ci Sun,[1] Xiaotian Li,[1] Bayanheshig,[1] and Jicheng Cui[1,*]

[1]National Engineering Research Centre for Diffraction Gratings Manufacturing and Application, Changchun Institute of Optics, Fine Mechanics and Physics, Chinese Academy of Sciences, Changchun Jilin 130033, China
[2]Daheng College, University of Chinese Academy of Sciences, Beijing 100049, China
*Corresponding author: jicheng_cui@163.com

Received 5 June 2018; revised 27 July 2018; accepted 27 July 2018; posted 30 July 2018 (Doc. ID 334314); published 23 August 2018

**A miniaturized portable short-wave infrared imaging spectroscopy optical system is designed based on a prism-grating dispersion module. We established a prism-grating model to calculate the optimal combination of prism and grating parameters to balance spectral smile over the entire band. The design method for the telescopic system and spectroscopic system combines independent design with integrated optimization. The system's spectral smile and spectral keystone are less than 15 μm and less than half a pixel, respectively. The total optical system length is 230 mm, which meets the miniaturization requirements for airborne systems. The system's spatial resolution is 1 mrad, and its average spectral resolution is 6.2 nm. The system offers the advantages of large relative aperture, excellent imaging quality, reduced spectral smile, and spectral keystone, miniaturization, and portability.** 

***OCIS codes:*** (220.0220) Optical design and fabrication; (300.6340) Spectroscopy, infrared; (120.4640) Optical instruments.

https://doi.org/10.1364/AO.57.0000F8

## 1. INTRODUCTION

An imaging spectrometer is an optical instrument that integrates imaging with spectroscopy [1,2]. Since first appearing in the early 1980s, after years of development, imaging spectrometers have been widely used in applications including remote sensing, medical detection and diagnosis, mineral resource exploration, environmental monitoring, military reconnaissance, and disguised identification [3–6]. Imaging spectrometers are generally divided into two types based on their different working bands: the visible/near-infrared type, which operates in the 400–1000 nm band, and the short-wave infrared type, which operates in the 1000–2500 nm band. Limited by the developmental status and cost of related technologies such as compatible optical materials and detectors [7,8], a smaller proportion of the research has focused on the short-wave infrared imaging spectrometers. However, with the rapid development of unmanned aerial vehicle (UAV) technology [9], the demand for miniaturized and portable short-wave infrared imaging spectrometers for UAV applications has become increasingly intense; therefore, research into the development of miniaturized and portable short-wave infrared imaging spectrometer technology is both important and urgently required.

As early as 1991, Vaarala *et al.* bonded a volume-phase holographic grating between two prisms to obtain a prism-grating-prism (PGP) dispersion module and developed a corresponding imaging spectrometer [10]. The imaging spectrometer that was based on this PGP dispersion module and use of a transmissive optical structure has characteristics that include small module volume and light weight, thus demonstrating potential for airborne operation. Because the prism and the grating have different dispersion characteristics [11,12], the PGP module can eliminate a portion of the spectral smile automatically. Unfortunately, while it is necessary to ensure that the optical system is coaxial, Aikio did not build a model to calculate the optimal combination of prism and grating parameters to maximize elimination of the spectral smile. In addition, the core technology of the PGP module is monopolized by the Specim company that was established by Aikio, thus restricting further popularization and application of this technology.

After the PGP concept was proposed, it was widely promoted and used in imaging spectrometers [13–15]. Many variant structures have also been derived, including the prism-grating (PG) module [16,17], which reduces both development difficulty and cost by removing a prism. Of course, because of the removal of the second prism, the optical axis of the optical system is deflected after the dispersion of the PG module. However, this deflection can be compensated via mechanical structure design, and there is no critical effect on the imaging quality or performance of the optical system. Yang from our laboratory designed a PG dispersion module for

operation in the band from 400 nm to 800 nm [16]. Based on this PG module, a prototype imaging spectrometer was developed successfully and demonstrated excellent performance [18]. Based on this prototype, we have completed the development of a visible/near-infrared PG imaging spectrometer with a 400–1000 nm operating range [19].

In this paper, we focus on the short-wave infrared wavelength band ranging from 1000 nm to 2500 nm. It should be pointed out that the application of the PG module in the short-wave infrared band is very different from that previously published in the visible near-infrared band, so it is not a simple migration. For example, most optical glasses do not have high optical transmittance in the short-wave infrared band; therefore, the types of optical materials that can be used in the design of the optical system are greatly limited. That is to say, compared with the visible near-infrared band, the short-wave infrared band can no longer use the prism material as a variable to optimize the spectral smile of the PG module. And the short-wave infrared band is invisible, so we need to consider the factors of the adjustment when designing. We have carried out a more rigorous tolerance allocation and analysis to ensure the relatively loose tolerance requirements of the system, so as to reduce the difficulty of adjustment. Based on the above considerations and previous research work, we have established a PG model to calculate the optimal combination of prism and grating parameters, and a complete optical system is designed for the imaging spectrometer based on the PG module. The final design result shows its value for practical applications.

## 2. PRINCIPLE

A schematic diagram of the short-wave infrared imaging spectrometer's optical system is shown in Fig. 1(a). The system includes the telescopic system and the spectroscopic system, of which the spectroscopic system forms the core part. The spectroscopic system includes a slit, a collimation group, a dispersion module, and a focusing group, of which the dispersion module represents the core part. In imaging spectrometers, selection of the dispersion module is the crucial step and often determines the structure of the entire optical system.

Prisms and gratings are commonly used as dispersion elements in imaging spectrometers. However, when prisms or gratings alone are used, the spectral lines of the optical system tend to bend because of nonprincipal section incidence [20]. The spectral smile is an intractable aberration that occurs in imaging spectrometers. The spectral smile increases the difficulty and complexity of spectral calibration of imaging spectrometers and also makes spectral data processing significantly more difficult [21]. Therefore, combined dispersion modules such as PGP and PG were proposed, which use the differing dispersion characteristics of the prisms and gratings to reduce the spectral smile of the optical system. In this work, a PG module is used as the dispersion module for the short-wave infrared imaging spectrometer.

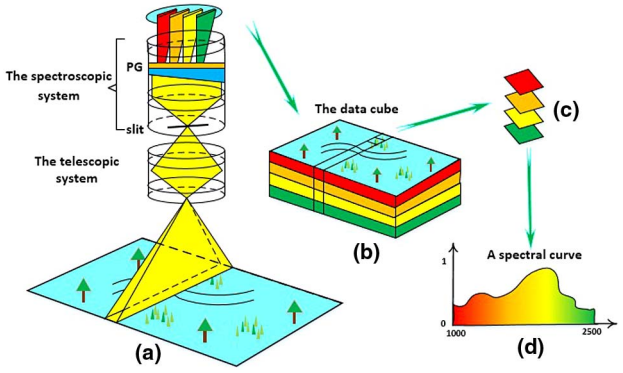


**Fig. 1.** Schematic diagram showing working principle of push-broom short-wave infrared imaging spectrometer system.

Airborne short-wave infrared imaging spectrometers often use the push-broom scan mode [22], and the working principle of this type of system is shown in Fig. 1(a). The reflected light from a ground target is imaged using the telescopic system via the slit that is located on the telescopic system's focal plane; the light thus enters the spectroscopic system through the slit. The incident light is then collimated into parallel light by the collimation group and subsequently dispersed using the PG module. After that, the parallel light is imaged by the focusing group located on the image surface and is finally received by the detector. We can therefore obtain the image and spectral information from the slit field, and we can expand the slit's field of view into a plane field of view using the push-broom scan of the spectrometer.

The data that are obtained by the imaging spectrometer are referred to as a data cube [23]. Figure 1(b) shows a schematic diagram of the data cube. This data cube contains all spatial image information and spectral information for the entire scanning range of the imaging spectrometer. Each data column in the data cube, as shown in Fig. 1(c), can be converted into a spectral curve for the spatial location that corresponds to a specific pixel, as shown in Fig. 1(d). The imaging spectrometer can therefore perform imaging and spectral analysis conveniently over a specific spatial range.

The standpoint of this instrument is to apply to the UAV system to study wheat scab. China is a big agricultural country, and most of the residents live on wheat, especially in northern China. Wheat scab is one of the main diseases of wheat, which can lead to dry seedlings, wheat straw rot, and even wheat ear rot, which will seriously affect the quality and yield of wheat. Based on the previous research and combined with the application background, the specific technical specifications required are shown in Table 1.

**Table 1. Requirement of Technical Specifications**

| Parameters | Value |
|---|---|
| Wavelength range | 1000 nm–2500 nm |
| Focal length | 30 mm |
| F-number | 2.4 |
| Spectral resolution | <10 nm |
| Field angle | >15° |
| Spatial resolution | 1 mrad |
| Spectral smile | <half a pixel |
| Keystone | <half a pixel |
| Optical length | <250 mm |

## 3. OPTICAL DESIGN

The design process for the short-wave infrared imaging spectrometer optical system includes telescopic system design, spectroscopic system design, and a combined design of these two systems. In this design process, under the premise of parameter matching, the telescopic system, and the spectroscopic system are designed independently. After these independent design processes, the two systems are combined, and on the basis of ensuring the independent performance of the two systems, the system parameters for integrated optimization are fine-tuned to provide further enhancement of the imaging quality of the entire optical system.

### A. Optical Design of the Telescopic System

The telescopic system is designed in the form of a telecentric path in image space to ensure that the main light in each field of view can be vertically incident on the slit in the spectroscopic system. The spatial resolution of the short-wave infrared imaging spectrometer is largely determined by the telescopic system properties. The technical index requires spatial resolution of 1 mrad, while the reduction ratio of the spectroscopic system is 1. We used a short-wave infrared focal plane detector with 320 × 256 pixels and a pixel size of 30 μm. The focal length of the telescopic system can thus be decided using the following:

$$1\ \text{mrad} = \frac{30\ \text{um}}{f}. \tag{1}$$

We obtained a value of $f = 30$ mm. At the same time, to ensure matching of the telescopic system to the spectroscopic system, the telescopic system's image size should be consistent with the slit length in the spectroscopic system. Because the reduction ratio of the spectroscopic system is 1, the slit length is the same as the spatial dimension of the detector. The spatial dimension of the detector is given by $L = 320 \times 30\ \mu\text{m} = 9.6$ mm, and thus the half-field angle of the telescopic system can be obtained as follows:

$$\omega = \arctan\left(\frac{L}{2f}\right) = 9.1°. \tag{2}$$

The field angle of the telescopic system is thus $2\omega = 18.2°$. The technical specifications of the telescopic system are listed in Table 2.

The initial optical structure of the telescopic system is determined by the system's focal length, F-number, and field angle. During the optimization process, the telecentric path in image space and the image size are used as constraints. Given that most optical glass has low transmittance at 2500 nm, virtual glass is used to optimize the optical path during the design process, and when this virtual glass is replaced with actual optical glass, the material transmittance factor becomes the main consideration. The 10 mm transmittance of all optical glass used at 2400 nm is more than 0.86. It can be calculated that the internal transmittance of optical glasses of the telescope system is $T_1 = 0.658$ at 2400 nm. During the optimization process, the system performance is evaluated using spot diagrams and the modulation transfer function (MTF). The final optical system shows excellent performance and meets the requirements detailed in the technical specifications.

**Table 2. Telescopic System Technical Specifications**

| Parameters | Value |
|---|---|
| Wavelength range | 1000 nm–2500 nm |
| Focal length | 30 mm |
| F-number | 2.4 |
| Field angle | ±9.1° |
| Spatial resolution | 1 mrad |

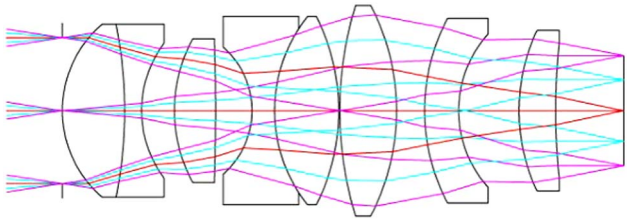

**Fig. 2.** Optical structure of the telescopic system.

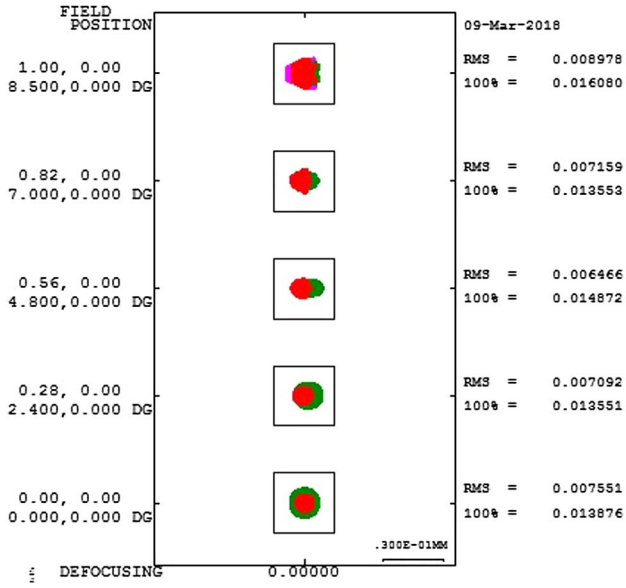


**Fig. 3.** Spot diagram of the telescopic system.

The optical structure of the telescopic system is shown in Fig. 2, and its length is 50 mm. The system's spot diagram is shown in Fig. 3. The diagram shows that the spots in each field of view are regular and are well focused within one pixel. The MTF curve of the telescopic system is shown in Fig. 4. Because the detector pixel size is 30 μm, the cutoff frequency is 16.7 l/mm. The curve shows that the MTF is higher than 0.8 for each field of view.

### B. Optical Design of Spectroscopic System

The spectroscopic system is the core section of the imaging spectrometer and determines the spectral resolution of the imaging spectrometer. The core part of this spectroscopic system is the dispersion module. Selection of the dispersion module determines the optical structure of the system. In this paper, a PG module is used as the dispersion module, and the spectral smile

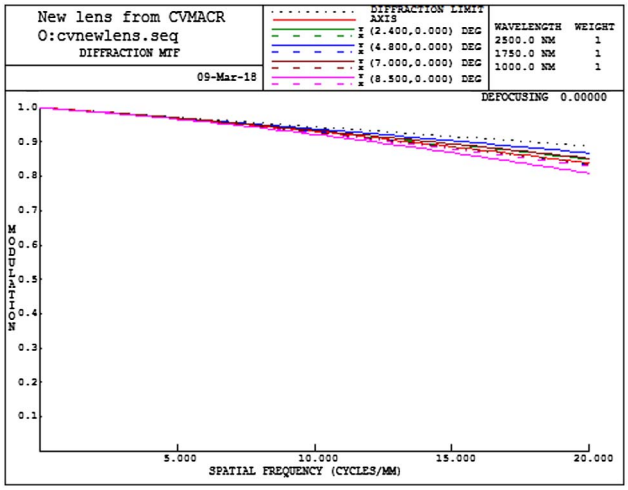


**Fig. 4.** MTF curve of the telescopic system.

across the entire working band is reduced by matching the prism parameters with the grating parameters. The collimation group and the focusing group, which are located before and after the PG module, respectively, use a symmetrical structure that is beneficial for the correction of system aberrations.

The grating used in the PG module has a density of 150 l/mm, and we used the −1 order in this system. The PG module shown in Fig. 5 was established for the short-wave infrared wavelength band from 1000 nm to 2500 nm. In Fig. 5(a), the $YOZ$ plane represents the meridional section of the PG module, and in Fig. 5(b), the $XOZ$ plane represents the sagittal section of the PG module. The nonprincipal section incident rays and the structural parameters of the PG module are used as the model inputs [16,18].

As shown in Fig. 5, $n_x$ is the refractive index of different materials, $\theta_t$ is the top angle of the prism, $\theta_s$ is the angle between the incident rays and the principal section, $\overrightarrow{P_x}$ is the unit normal vector of each media interface, and $\overrightarrow{Q_x}$ is the unit vector of light in each medium. From the geometric relationship in Fig. 5, we can get

$$\overrightarrow{Q_0} = (-\sin\theta_s, 0, \cos\theta_s), \tag{3}$$

$$\overrightarrow{P_1} = (0, -\sin\theta_t, \cos\theta_s). \tag{4}$$

Therefore, the incident angle $\theta_1$ at interface 1 is

$$\theta_1 = \arccos(\overrightarrow{Q_0} \cdot \overrightarrow{P_1}). \tag{5}$$

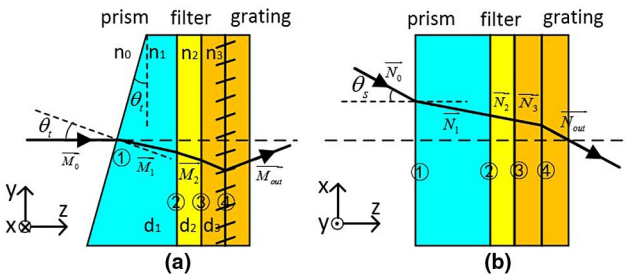


**Fig. 5.** Schematic diagram of the PG module.

According to the law of refraction, the refraction angle is as follows:

$$\theta_1' = \arcsin\left(\frac{n_0}{n_1}\sin\theta_1\right). \tag{6}$$

Then, according to the law of refraction in vector form, we can get

$$n_1\overrightarrow{Q_1} - n_0\overrightarrow{Q_0} = T\overrightarrow{P_1}, \tag{7}$$

$$T = n_1\cos\theta_1' - n_0\cos\theta_1. \tag{8}$$

We can get

$$\overrightarrow{Q_1} = \frac{n_0\overrightarrow{Q_0} + (n_1\cos\theta_1' - n_0\cos\theta_1)\overrightarrow{P_1}}{n_1}. \tag{9}$$

It can also be obtained from Fig. 5:

$$\overrightarrow{P_2} = (0, 0, 1), \tag{10}$$

$$\overrightarrow{P_2} = \overrightarrow{P_3} = \overrightarrow{P_4}. \tag{11}$$

By means of Eqs. (3)–(11) cyclic calculations, $\overrightarrow{Q_2}$ and $\overrightarrow{Q_3}$ can be sequentially obtained. $\overrightarrow{Q_3}$ is the incident light of the grating. We can obtain the −1 order diffraction light $\overrightarrow{Q_{\text{out}}}$ by the grating equation. Therefore, we can get the angle $\varphi(\theta_s)$ between the projection of the ray $\overrightarrow{Q_{\text{out}}}$ in the principal section and the grating normal line $\overrightarrow{P_4}$. Obviously, the incidence angle $\theta_s$ of the nonprincipal section will directly affect $\varphi(\theta_s)$. The incident angle $\theta_{s\_\max}$ corresponding to the incident ray at the end of the slit is the maximum, and the corresponding angle is $\varphi_{\max}$. The incident angle $\theta_{s\_\min}$ corresponding to the incident ray at the center of the slit is the minimum, and the corresponding angle is $\varphi_{\min}$. Obviously, $\varphi_{\max}$ and $\varphi_{\min}$ are different, which leads to the spectral smile of the system. And we can get the spectral smile $\Delta l$ by

$$\Delta l = f\cdot(\varphi_{\max} - \varphi_{\min}), \tag{12}$$

where $f$ is the focal length of the imaging group. By taking the spectral smile of the entire wavelength band into consideration, the prism top angle is finally determined.

It should be noted that many factors in the actual optical structure will affect the value of the spectral smile, and the prism and grating parameters obtained via theoretical calculations simply allowed determination of a good initial structure. In the subsequent design process, we used this initial structure in combination with the optical system to allow further optimization. The spectroscopic system specifications are listed in Table 3.

During the design process, the focusing group, which is designed in the form of a telecentric path in object space, is designed first, and, after optimization, an inversion of the focusing group is then used as the collimating group, so the collimating group is a telecentric path in image space. Then, the collimating group and the focusing group are combined for further optimization. Finally, the PG module is inserted into the collimating group and the focusing group to form the complete spectroscopic system. And we can calculate the internal

**Table 3. Spectroscopic System Technical Specifications**

| Parameters | Value |
|---|---|
| Focal length | 30 mm |
| F-number | 2.4 |
| Wavelength range | 1000 nm–2500 nm |
| Average spectral resolution | 6.2 nm |
| Slit width | 30 um |
| Prism top angle | 16.25° |
| Grating groove density | 150 l/mm |

transmittance of optical glasses of the spectroscopic system as $T_2 = 0.512$ at 2400 nm. The final optimization of the resulting spectroscopic system is based on constraints including the spot diagram, the MTF, the spectral smile, the spectral keystone, and the image size.

The optical structure of the spectroscopic system is shown in Fig. 6, and the system's length is 50 mm. The figure shows that the collimation group and the PG module are located on the same optical axis. After the PG module, the optical axis is deflected, i.e., the optical axis of the collimation group and the PG module is at an angle with respect to the optical axis of the focusing group; in this design, that angle is 8°. The spot diagram is shown in Fig. 7 and shows that the spots in each field of view are all well focused within a single pixel. Figure 8 shows the MTF curve for the central wavelength of 1750 nm. The figure shows that the MTF for the entire field of view is higher than 0.8 at 16.7 l/mm.

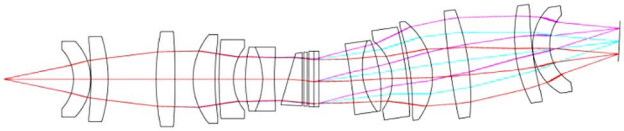

**Fig. 6.** Optical structure of the spectroscopic system.

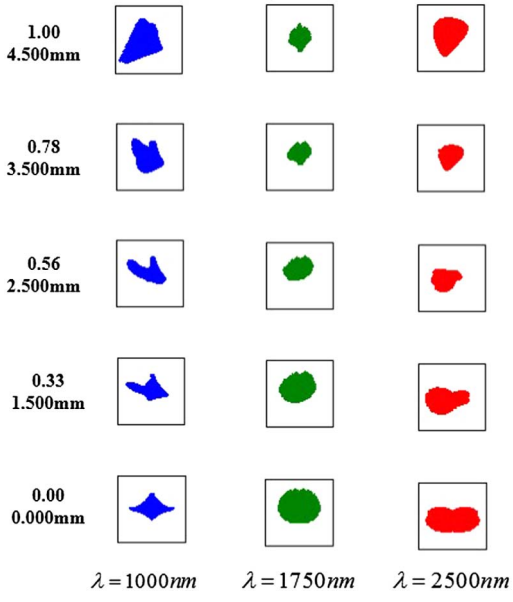


**Fig. 7.** Spot diagram of the spectroscopic system.

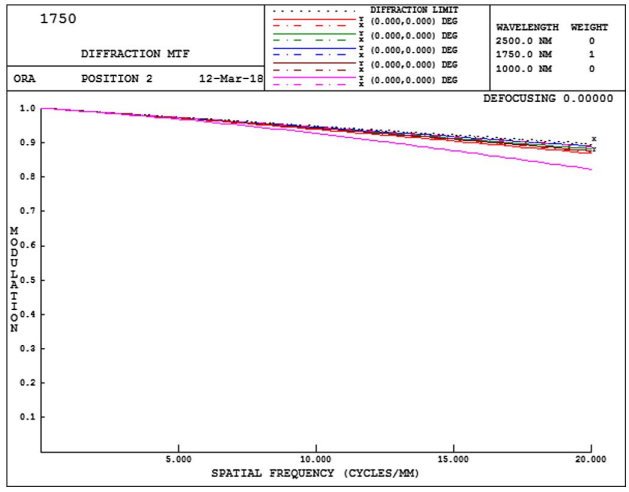


**Fig. 8.** MTF curve of the spectroscopic system.

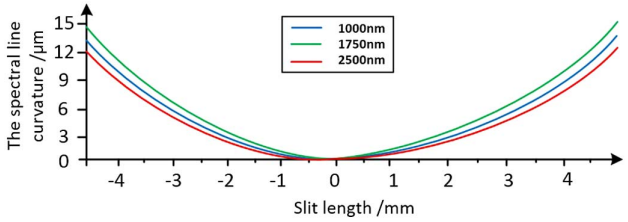


**Fig. 9.** Schematic diagram of spectral smile of the spectroscopic system.

As part of the design results for the spectroscopic system, in addition to the spots and the MTF, it is also necessary to examine the values of the spectral smile and the spectral keystone. We obtained the spectral smile and spectral keystone values of the system via real ray tracing. Figure 9 shows a schematic diagram of the spectral smile of the spectroscopic system. The diagram shows that the spectral smile in the 1000–2500 nm wavelength range is less than 15 μm, which is less than half a pixel. The spectral keystone of the system is also less than 15 μm throughout the entire wavelength band, and the distortion rate is approximately 1.7‰. The spectral smile and the spectral keystone are both less than half a pixel, meaning that no correction is required for data processing, which thus reduces the data processing difficulty and reduces the workload. We need to point out that a spectral smile of 15 μm is not the state of the art. However, considering that the purpose of designing the system is practical application, we have not further optimized it in order to maintain the loose tolerance requirement. Of course, the spectral smile can be optimized to smaller if needed.

### C. Integrated Optimization of Optical System

After the telescopic system and the spectroscopic system have been independently designed, further combinatorial optimization of the two systems is required. However, because the telescopic system and the spectroscopic system have different characteristics, their respective performances must not be

destroyed during the process of combinatorial optimization. In other words, it is necessary to balance the combinatorial aberrations based on the premise that the two systems can maintain good performance when they work independently. We call this process the integrated optimization of the imaging spectrometer's optical system.

The telescopic system and the spectroscopic system both have the same F-number, and their apertures are matched, so the two systems can be combined perfectly. The aberration distributions of the telescopic system and the spectroscopic system are analyzed, and while the combination of the two systems can offset some of these aberrations, some of the remaining aberrations simultaneously accumulate. We mainly consider the aberrations that would accumulate after combination of the two systems and adjust the system parameters to ensure that the sizes of these aberrations after combination of the systems remain within the allowable range.

The optical transmittance of the entire system can be decided by the internal transmittance of optical glasses of the telescope system, that of the spectroscopic system, the transmission coefficient after reflection from the optical surface, and the diffraction efficiency of the grating. The optical elements will be coated with anti-reflection coating on the surface, and the transmissivity of a single surface can be guaranteed to be over 0.995. The optical system has a total of about 40 faces, so the transmission coefficient after reflection from the optical surface is about $T_R = 0.995^{40} = 0.818$. The grating we choose is a volume phase holographic grating with relatively high diffraction efficiency. The average diffraction efficiency in the whole working band is about $E = 0.65$. So far, we can estimate the optical transmittance of the entire system as $T = T_1 \times T_2 \times T_R \times E = 0.178$. And these data are at 2400 nm, which is almost the worst position in the entire band, so the transmittance at other wavelengths will be obviously higher than this. Back to our application background, the instrument will research wheat scab in sunny outdoors, with sufficient illumination, so this design can well meet the needs of the application.

We have taken some measures to reduce the system's stray light. A 1000–2500 nm bandpass filter is installed at the forefront of the telescope system to suppress other wavelengths of light from entering the optical system, and a gradient filter is installed before the detector to suppress stray light (including other orders of light) into the detector. Of course, it should be pointed out that the above measures are the most basic. In the future, we will perform detailed stray light analysis of the system and carry out targeted elimination.

The optical structure of the PG short-wave infrared imaging spectrometer system is shown in Fig. 10. The figure shows that the system's aperture stop is located on the first surface of the telescopic system and that the distribution of the optical elements is balanced over the entire system, which allows sufficient space for the mechanical design. The spot diagram of the PG short-wave infrared imaging spectrometer system is shown in Fig. 11. The diagram shows that the spots in each field of view are all focused within one pixel. As shown in Fig. 12, we carried out the MTF tolerance analysis/s for the central wavelength of 1750 nm to test the tolerance sensitivity of the optical system and thus determine the feasibility of practical application of this system in the development of the instrument. The results of the tolerance analysis show that under the default tolerance allocation conditions, the MTF of the system has a

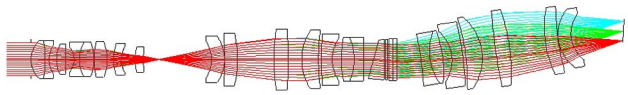

**Fig. 10.** Optical structure of the PG short-wave infrared imaging spectrometer system.

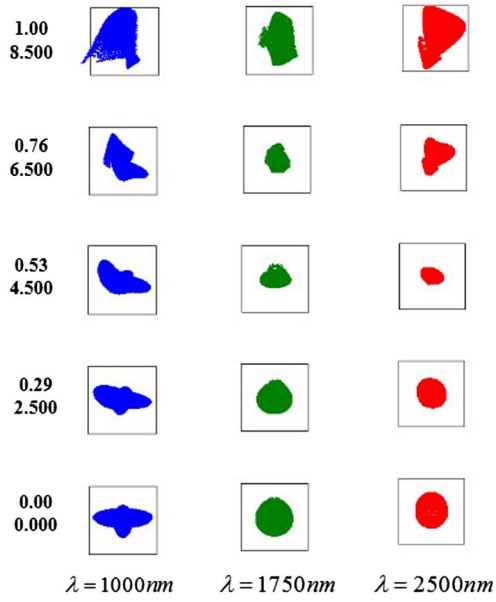


**Fig. 11.** Spot diagram of the PG short-wave infrared imaging spectrometer system.

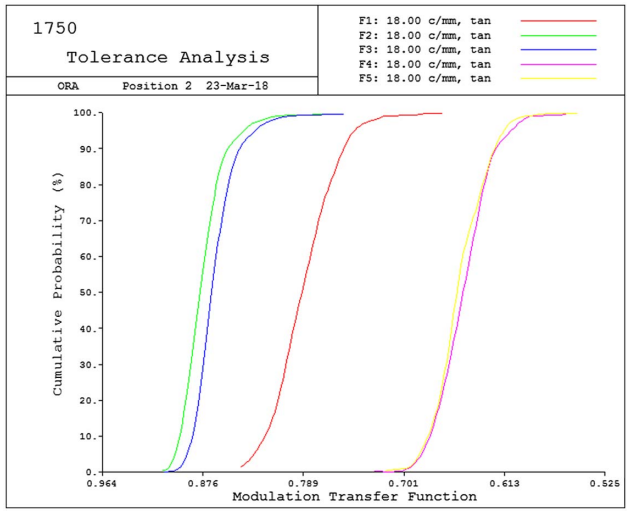


**Fig. 12.** MTF tolerance analysis of the PG short-wave infrared imaging spectrometer system.

probability of 99% above a value of 0.6, which meets the requirements for practical application of the system.

## 4. CONCLUSIONS

In this paper, a short-wave infrared imaging spectrometer is designed based on a PG module. We have optimized the prism and grating parameters using modeling calculations to balance the spectral smile over the entire system operating band from 1000 nm to 2500 nm. We adopted an independent design and integration optimization method for design of the telescopic system and the spectroscopic system. While ensuring that the independent performances of the telescopic system and the spectroscopic system were maintained, we fine-tuned the system parameters to balance the aberrations of the telescopic system and those of the spectroscopic system to improve the overall performance of the entire optical system. The design results show that the performance of the resulting short-wave infrared imaging spectrometer optical system is excellent. The layout of the optical elements ensures that sufficient space remains for the mechanical design, and we have fully considered both the feasibility and the reliability of the optical system. The spot sizes of the system are all less than 30 μm, thus ensuring that the energy is all concentrated in one pixel, and the MTF of the default tolerance limit is greater than 0.6. The spectral smile and the spectral keystone of the system are both less than 15 μm, which is less than one half of the pixel size. Therefore, the designed short-wave infrared imaging spectrometer optical system, which is based on the PG dispersion module, meets the practical application requirements.

**Funding.** National Major Scientific Instrument and Equipment Development Projects (2014YQ120351); Chinese Finance Ministry for the National RD Projects for Key Science Foundation of China (NSFC) (61505204); Ministry of National Science and Technology for National Key Basic Research Program of China (2014CB049500); Changchun Science and Technology Project (12ZX23); Jilin Major Province Science Technology Development Program Project (20140203011GX).

## REFERENCES

1. R. O. Green, M. L. Eastwood, and C. M. Sarture, "Imaging spectroscopy and the airborne visible/infrared imaging spectrometer (AVIRIS)," Remote Sens. Environ. **65**, 227–248 (1998).
2. R. M. Sullenberger, A. B. Milstein, and Y. Rachlin, "Computational reconfigurable imaging spectrometer," Opt. Express **25**, 31960–31969 (2017).
3. E. Bendor, S. Chabrillat, and J. A. M. Demattê, "Using imaging spectroscopy to study soil properties," Remote Sens. Environ. **113**, S38–S55 (2009).
4. T. Wu, G. Li, and Z. Yang, "Shortwave infrared imaging spectroscopy for analysis of ancient paintings," Appl. Spectrosc. **71**, 977–987 (2017).
5. J. C. Cui, Y. G. Tang, P. Han, M. Z. Pan, and J. N. Zhang, "Development of diagnostic imaging spectrometer for tumor on-line operation," Opt. Precis. Eng. **21**, 3043–3049 (2013).
6. L. Hang, N. Liao, and H. Li, "High resolution ultraviolet imaging spectrometer for latent image analysis," Opt. Express **24**, 6459–6468 (2016).
7. X. Sun, J. B. Abshire, and J. D. Beck, "HgCdTe avalanche photodiode detectors for airborne and spaceborne lidar at infrared wavelengths," Opt. Express **25**, 16589–16602 (2017).
8. P. Chorier, P. M. Tribolet, and A. Manissadjian, "Application needs and trade-offs for short-wave infrared detectors," Proc. SPIE **5074**, 363–373 (2003).
9. S. Hu, G. H. Goldman, and C. C. Boreldonohue, "Detection of unmanned aerial vehicles using a visible camera system," Appl. Opt. **56**, B214–B221 (2017).
10. T. Vaarala, M. Aikio, and H. Keraenen, "Advanced prism-grating-prism imaging spectrograph in online industrial applications," Proc. SPIE **3101**, 322–330 (1997).
11. S. Zhu, M. Tang, and Y. Ji, "Optical design of prism-grating-prism imaging spectrometers," Acta Photon. Sin. **7156**, 2270–2273 (2009).
12. C. W. Dirk, M. F. Delgado, and M. Olguin, "A prism-grating-prism spectral imaging approach," Stud. Conserv. **54**, 77–89 (2013).
13. E. Herrala, J. T. Okkonen, and T. S. Hyvarinen, "Imaging spectrometer for process industry applications," Proc. SPIE **2248**, 33–40 (1994).
14. P. B. Garcia-Allende, O. M. Conde, and J. Mirapeix, "Data processing method applying principal component analysis and spectral angle mapper for imaging spectroscopic sensors," IEEE Sens. J. **8**, 1310–1316 (2008).
15. H. Zhang, T. Wu, and L. Zhang, "Development of a portable field imaging spectrometer: application for the identification of sun-dried and sulfur-fumigated Chinese herbals," Appl. Spectrosc. **70**, 879–887 (2016).
16. Z. P. Yang, Y. G. Tang, and Bayanheshig, "Optimization design method for optical system of prism-grating ultraspectral imaging spectrometers," Acta Opt. Sin. **34**, 0911003 (2014).
17. H. Chen, Y. Gong, and C. Luo, "Design of prism-grating imaging spectrometer with eliminating spectral smile," Acta Opt. Sin. **34**, 0922004 (2014).
18. Z. P. Yang, "*Optimization Design Method and Integration Technology for Prism-Grating Hyperspectral Imaging Spectrometer*," (Changchun Institute of Optics, Fine Mechanics and Physics, CAS, 2015).
19. J. Yang, R. Zhang, M. Z. Pan, and J. C. Cui, "Optical design of PG imaging spectrometer with large aperture and surface field," Opt. Precis. Eng. **25**, 335–342 (2017).
20. X. L. Zhang, Y. Liu, Q. Sun, C. Li, and H. Zhou, "Design of long-wave infrared imaging spectrometer with eliminating spectral curvature," Opt. Precis. Eng. **22**, 266–273 (2014).
21. L. Feng, "Spectral curvature correction method based on inverse distance weighted interpolation," Proc. SPIE **10004**, 100041W (2016).
22. J. Jemec, F. Pernuš, and B. Likar, "Deconvolution-based restoration of SWIR push-broom imaging spectrometer images," Opt. Express **24**, 24704–24718 (2016).
23. Y. Luo, N. Liao, and X. Wang, "Fast processing of imaging spectrometer data cube based on FPGA design," Proc. SPIE **6787**, 678708 (2007).